Promoting rotation, friction, and mixed lubrication for particles rolling on microstructured surfaces

Brian K. Ryu, Richard J. Hommel, Paul Roberts, and Joëlle Fréchette

Promoting rotation, friction, and mixed lubrication for particles rolling on microstructured surfaces

Brian K. Ryu, Richard J. Hommel, Paul Roberts and Joëlle Fréchette*

Department of Chemical and Biomolecular Engineering, Johns Hopkins University, Baltimore, Maryland 21218, United States

* Corresponding author. Telephone: (410) 516-0113. Fax: (410) 516-5510. E-mail: jfrechette@jhu.edu.

ABSTRACT

We investigate how the aspect ratio of micropillar or microwell arrays patterned on a surface affects the rolling and slipping motion of spheres under flooded conditions at low Reynolds numbers. We study arrays of rigid microstructures with aspect ratios varying over two orders of magnitude for surface coverages ranging from 0.04 to 0.96. We investigate how the surface features (dimensions, surface coverage, and geometry) individually impact the motion of the sphere. We find that increasing microstructure height results in higher rotational velocities on all studied surfaces. We then model the motion of the spheres using two physical parameters: an effective separation and a coefficient of friction between the sphere and the incline. We find that a simple superposition of resistance functions, previously shown to accurately predict the motion of spheres for different surface coverages and geometries, indeed shows good agreement with experimental outcomes for all microstructure heights studied. We also perform separate sliding friction measurements via a force microscope to measure the coefficient of friction between the sphere and incline, under identically flooded conditions. A comparison of the sliding friction measurements at different Hersey numbers suggests that the effect of the microstructure on the coefficient of friction becomes more important as the Hersey number increases.

I. INTRODUCTION

Nature provides many examples where surface topography mediates adhesion and friction, for example the intricate features observed on the toe pad of insects such as beetles or crickets allow them to climb on a wide range of surfaces [1-4]. Similarly, the toe pads of the tree frogs consist of hexagonal arrays of soft microposts separated by narrow channels to provide traction under wet or flooded conditions [5,6]. As a result, bio-inspired surface structures have been developed to enhance adhesion and friction under lubricated conditions for applications in transportation, robotics, or manipulation of electronics components [7,8]. The effect of surface texturing as a means to control lubricated friction has also been investigated extensively [9-11]. Surface microstructures lead to non-conformal contacts and qualitatively alter the Stribeck curves that delineate the lubrication regimes according to the Hersey number ($\lambda = \eta u/P$, where η is the dynamic viscosity, u is the translational velocity, and P is the applied normal load) [12]. In particular, experiments showed that surface microstructure can extend the hydrodynamic lubrication regime, where the load is fully supported by the fluid, to lower sliding velocities [13]. Other experiments also showed the opposite: an increase in friction in the presence of surface microstructures. These experiments suggest that the mixed lubrication regime, where the load is supported by solid-solid contacts as well as by the fluid, is extended to higher sliding velocities in the presence of surface microstructures [14]. Therefore, the question remains as to what are the mechanisms leading to an increase (or decrease) in friction in the presence of microtextured surfaces. More specifically a relationship between surface structure, hydrodynamics, and friction is still lacking and would help develop design guidelines to engineer materials with engineered interfaces.

Surface microstructure also influences the rolling motion of a particle on a surface in a viscous fluid, where again a delicate balance of friction, hydrodynamics, and surface topography determines the extent of rotation and sliding. A distinguishing feature of a study of rolling motion from the more common hydrodynamic lubrication or friction force measurements of normal drainage [15-17] or lateral sliding [18] is the presence of a torque due to normal-tangential coupling. The rolling motion of a particle on a surface is also ubiquitous during the detachment and re-entrainment of particles adhered on a surface [19,20], cells in blood vessels or on tissues roll on rough surfaces [21,22], and on bearings common in tribological testing [23]. Therefore, a better understanding of how the rolling motion of particles is modulated by surface microstructure could help engineer materials' interfaces that favor either rotation or sliding.

To study rolling motion on a microstructured surface, the motion of a sphere down an incline in a viscous fluid requires independent measurements of the rotation and sliding velocities, as illustrated in Figure 1. Earlier studies followed this approach and examined the motion of spheres on a rough incline, and the problem was analyzed quantitatively for the case where the roughness elements were randomly dispersed and dilute [24,25]. In contrast to surfaces with sparse and random roughness, many organisms found in nature, as well as microtextured surfaces for tribological applications, systematically utilize well-designed and unique structures at high surface coverages. Several past studies have investigated individually the normal motion [15,17] and lateral motion [26] of spheres near microtextured surfaces. However, there are still no systematically established quantitative relationships between the effect of microstructure on the sliding or rolling motion of a sphere in a viscous fluid. More specifically, mixed lubrication, where the load is distributed between the fluid pressure and solid-solid contacts, is a regime that can be difficult to quantify and the role of microstructures under mixed or hydrodynamic lubrication is poorly understood [27-31]. In addition, studying the motion of a rolling sphere down a microstructured incline could serve as a simple quantitative tribological measurement in the mixed lubrication regime, and provide a means to understand how surface topography alters the coupling between hydrodynamics and friction (see Figure 1).

Previously, we proposed a model that implements a simple superposition of hydrodynamic resistance forces and torques to characterize the rolling motion of spheres on non-dilute, periodic microstructured surfaces [32]. The resulting superposition model provides a first-order approximation of the rolling motion of a sphere on a microstructured surface. In the model the rolling sphere is characterized by an effective separation based on the microstructure height and surface roughness as well as by a coefficient of friction with the solid surface. Although in our prior work the superposition model predicted well the behavior of rolling spheres on periodically structured surfaces, the study was preliminary and undertaken for a single feature height. A study using varying microstructure aspect ratios to separate the diameter and height length scales is necessary to validate the scope of the model. Moreover, we did not situate the coefficient of friction obtained from comparing the model to the experiments to measurements of lubricated friction.

Our objectives in the current study are two-fold: 1) we aim to test the validity of the simple superposition model over a broader range of parameters, more specifically for features with aspect ratios that vary over two orders of magnitude, and 2) we seek to draw parallels between the apparent coefficients of friction obtained from fitting the experimental data to independent sliding

friction measurements obtained under lubricated conditions. To do so, we study the motion of rolling spheres on surfaces decorated with microscale features that span a comprehensive parameter space to cover a broad range of microstructure height, coverage, and geometry. More specifically, we examine the rotational and translational motion of smooth spheres on surfaces patterned with micropillars and microwells to compare and contrast the effect of topographical features on the sphere velocities, effective gap height, and apparent coefficients of friction. We also report on independent sliding friction measurements at varying Hersey numbers and show that the presence of microstructures does not impact friction at low Hersey numbers (in or near the boundary lubrication regime) and that microstructures effectively extend the mixed lubrication regime to higher velocities (when compared to a flat surface). Our results demonstrate that microstructures can be engineered to tune frictional behaviors at specific lubrication modes.

The remainder of this study is organized as follows: in Section II, we briefly present the model developed in our prior work [32], which we test the scope and validity of in the current study. We present protocols for fabrication of microstructures and methodology of rolling experiments as well as friction measurements via our multifunciontal force microscope in Section III. Our results, presented in Section IV, are divided into two parts. In Section IV.A, we show the effect of feature height on the rolling velocity of spheres by testing the model over a wide range of microstructure dimensions. Section IV.B discusses a detailed investigation of friction measurements on microstructured surfaces to connect friction experienced by spheres to the lubrication regimes of the Stribeck curve. The study concludes in Section V.
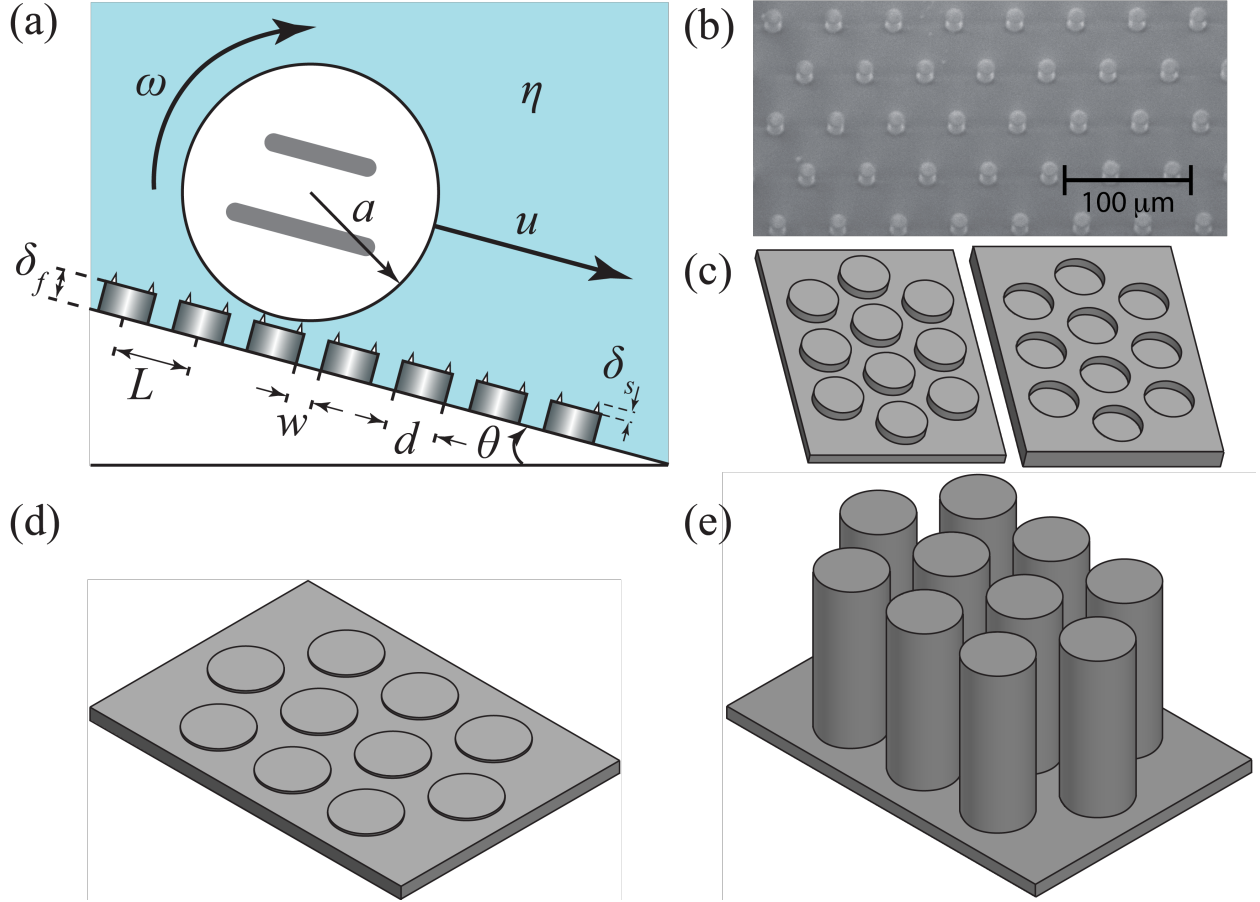
FIG 1. Experimental setup and microstructure characterization. (a) Sketch of a smooth sphere of radius a rolling with a translational velocity u and a rotational velocity ω on a microstructured incline submerged in a fluid of dynamic viscosity η. The variable incline has an angle of inclination θ and the microstructured surface has a feature height of δ_f, diameter d and spacing w. The top plane of the microstructures possesses an inherent roughness of δ_s. The two distinct parallel lines drawn on the side of the spheres allows tracking of angular orientation of the sphere. (b) SEM micrograph of an SU-8 micropillar array ($d = 10$ μm, $w = 40$ μm, $\phi = 0.04$). (c) Schematic of hexagonal arrays of micropillars (left) and microwell (right). (d) Schematic of low aspect ratio (0.04) array of micropillars. (e) Schematic of high aspect ratio (2.5) array of micropillars.

II. BACKGROUND

A. Motion of a Sphere on a Rough Incline

We consider the motion of a smooth, non-colloidal sphere of radius a, density ρ_p immersed in a Newtonian fluid of density ρ_f, dynamic viscosity η, and kinematic viscosity ν. The sphere is rolling down an inclined plane of angle of inclination θ with an angular velocity of ω and net translational velocity u at low Reynolds number (see Figure 1). To describe the motion, we follow the treatments from Smart *et al.*, which we only summarize here for clarification [24]. The Reynolds number of the motion is small, so that inertial forces are negligible. Further, we assume we are in the Stokes flow limit, and ignore colloidal interactions and other sources of

irreversibilities. The sphere is negatively buoyant with a density difference of $\Delta\rho$. Thus, the equations of motion become linear, and the dimensionless translational and rotational velocity of the rolling sphere simplify to:

$$U = \Omega = \frac{1}{F_T^* + F_R^* + \frac{4}{3}(T_T^* + T_R^*)} \tag{1}$$

for low angles of inclinations at which the sphere is purely rotating. In Eq. (1) the rotational and translational velocities are rendered dimensionless as $U = u/U_s \sin(\theta)$ and $\Omega = a\omega/U_s \sin(\theta)$, where U_s is the Stokes settling velocity, $U_S = \frac{2}{9}(a^2 g \Delta\rho/\eta)$, and F_T^*, F_R^*, T_T^*, and T_R^* are dimensionless resistance functions describing the hydrodynamic forces and torques acting on the sphere by the liquid. When θ is sufficiently high, the sphere rolls and slips and the velocity becomes:

$$\Omega = \frac{1 - \mu_f \cot(\theta)\left[1 + \frac{3}{4}F_T^*/T_T^*\right]}{F_R^* - T_R^* F_R^*/T_T^*}, \tag{2}$$

$$U = \frac{\frac{3}{4}\mu_f \cot(\theta) - \Omega T_R^*}{T_T^*}, \tag{3}$$

where μ_f is the coefficient of friction between the sphere and incline. The criterion for slipping is:

$$\cot(\theta) < \frac{\frac{4}{3}(T_T^* + T_R^*)}{\mu_f\left[F_T^* + F_R^* + \frac{4}{3}(T_T^* + T_R^*)\right]}. \tag{4}$$

In Eqs. (1)-(4), we assume that the coefficients of rolling and slipping friction are the identical. While numerical solutions of these dimensionless resistance functions were established by Dean and O'Neill, Goldman *et al.* developed the following analytical expressions in the case of a sphere asymptotically close to a plane wall with separation δ [33-35]:

$$F_T^*(\delta) = -\frac{8}{15}\ln\left(\frac{\delta}{a}\right) + 0.9588, \tag{7}$$

$$F_R^*(\delta) = \frac{2}{15}\ln\left(\frac{\delta}{a}\right) + 0.2526, \tag{8}$$

$$T_T^*(\delta) = \frac{1}{10}\ln\left(\frac{\delta}{a}\right) + 0.1895, \tag{9}$$

$$T_R^*(\delta) = -\frac{2}{5}\ln\left(\frac{\delta}{a}\right) + 0.3817. \tag{10}$$

The above model, developed by Smart *et al.*, assumes that the roughness features on the spheres merely act as asperities that provide a constant separation δ between the sphere and the plane, and that the surface coverage of the roughness elements is sparse enough that the hydrodynamic interaction between the roughness elements and the plane is negligible [24].

We note that the applicability of this framework depends on the range of separation that well-described by the hydrodynamic resistance functions in Eqs. (7) – (10). These analytical expressions are only valid for sufficiently small δ/a, and a comparison with exact numerical solutions provided by Goldman *et al.* shows that these logarithmic asymptotic solutions start to deviate for separations greater than 2% of the sphere radius [35].

B. Motion of a Sphere on a Microstructured Incline

Prior analysis by Smart *et al.* and Galvin *et al.* focused on randomly dispersed dilute roughness elements with negligible hydrodynamic interactions between the asperities and incline [24,36]. In our prior work [32], we developed an approximation inspired by the work of Staben *et al.*, which modeled the motion of a sphere between two parallel plane walls by adding the interactions between the sphere and each wall [37]. The treatment for this approximation is shown here for clarity only. We considered a microtextured incline with well-defined topography and a non-dilute solid area fraction ϕ, which we defined as the solid area fraction of the top plane of the microstructures.

In the non-dilute case, the interaction between the surrounding fluid and the microstructures can no longer be neglected, as the microstructures occupy a significant fraction of the volume between the rotating sphere and the plane incline. Hence our previous work provided a first order approximation of the interactions from two planes that are both asymptotically close to the rolling sphere yet maintain different separations. We treat the effect of two planes as a result

of a single predicted "effective" plane of height δ_pred. For a sphere near a plane with microstructures of height δ_f and an inherent roughness of the top plane of δ_s, we superimpose the resistance forces and torques from each plane weighed by the solid area fraction as the following:

$$\xi^*(\delta_{pred}) = \phi\xi^*(\delta_s) + (1 - \phi)\xi^*(\delta_f), \tag{11}$$

where ξ^* represents individual resistance forces and torques $(F_T^*, F_R^*, T_T^*, \text{ and } T_R^*)$ in Eqs. $(7) - (10)$. The first term on the right-hand side of Eq. (11) represents the resistance exerted on the sphere by the top plane of the microstructures, and the second terms represent the resistance contribution from the plane below the microstructures. Since these resistance functions are based on the expressions by Goldman *et al.*, both the inherent roughness of the top plane δ_s and the height of the microstructures δ_f must be sufficiently small compared to the sphere radius a [35].

Substituting Eq. (11) into Eqs. $(7) - (10)$ results in the following power-law expression for a predicted dimensionless effective gap width δ_{pred}/a:

$$\frac{\delta_{pred}}{a} = \left(\frac{\delta_s}{a}\right)^{\phi} \left(\frac{\delta_f}{a}\right)^{1-\phi}. \tag{12}$$

The predicted gap width, δ_pred, in Eq. (12) can be interpreted as an effective separation from the bottom surface experienced by the rotating sphere. We note here that δ_pred is dimensional and δ_pred/a is dimensionless. At the dilute limit, this expression predicts the effective gap δ_pred to be approximately equal to δ_f. However, as the solid fraction of the microstructures increases, the effective separation rapidly decreases, reaching δ_s for $\phi \to 1$. This superposition model is a first-order approximation that relates the coverage of microstructures to the apparent gap but neglects any geometrical effects of the microstructures. Hence, this analysis predicts that the effective gap width of arrays of micropillars and microwells should be the same at equivalent surface coverage ϕ and that the two surfaces are indistinguishable. An objective of our experiments is to test the validity of Eq. (12).

We note that to avoid ambiguities on the physical interpretation of ϕ, the area fraction of the top of the surface, we define the solid area fraction of hexagonal micropillar arrays with a diameter of d and spacing of w as:

$$\phi = \frac{\pi d^2}{2\sqrt{3}(d + w)^2},$$ (13)

where the highest possible coverage limited by the geometry is $\phi = 0.907$. The solid area fraction for hexagonal microwell arrays is:

$$\phi = 1 - \frac{\pi d^2}{2\sqrt{3}(d + w)^2}.$$ (14)

We note there that because we are interested in the area fraction of the top plane of microstructures, ϕ for microwells describe the connected area between wells (i.e. the void area fraction would be 1-ϕ). The inverted nature of microwell arrays with respect to micropillars result in a lowest possible coverage of $\phi = 0.093$.

III. MATERIALS AND METHODS
A. Ceramic Spheres

We used silicon nitride (Si_3N_4) ball bearings of density 3.29 g/cm^3 with diameters of 3.00 mm and 5.00 mm. The ball bearings (BC Precision) were of grade 5 with a maximum absolute roughness of 20 nm and a measured average absolute roughness R_a of less than 5 nm under a profilometer (Dektak). To track angular orientations of spheres during experiments, we drew two parallel lines of different lengths on the spheres (Figure 1(a)).

B. Fabrication of SU-8 Features

We constructed flat and microstructured surfaces with layers of SU-8 on silicon wafers following standard photolithography protocols. Prior to fabrication, we dehydration-baked each wafer at 200°C for 5 minutes. To initially create a flat base layer, we spin-coated a negative photoresist (SU-8 2007, MircoChem) onto the silicon wafer at 1700 rpm for 30 seconds. After spin-coating, we baked the wafer at 95°C for 3 minutes and then exposed to an energy of 140 mJ/cm^2 without a photomask. The exposed wafer was again baked at 95°C for 3 minutes. This protocol resulted in a flat basecoat of SU-8 with a thickness of 10 μm.

To construct microstructured surfaces, we spin-coated an additional layer of SU-8 on top of the basecoat. To achieve feature heights of 400 nm, 2 μm, 10 μm, and 25 μm, we used different

fabrication conditions respectively. Here, we briefly summarize the parameters used to obtain a feature height of 400 nm. On a dehydrated wafer, we spin-coated SU-8 2000.5 negative photoresist at 1200 rpm for 30 seconds with an acceleration of 500 rpm/s. We then baked the spin-coated wafer at 95°C for 2 minutes and followed by an exposure to an energy of 50 mJ/cm^2. We baked the exposed wafer again at 95°C for 2 minutes and then immersed in SU-8 developer (MicroChem) for 65 seconds. Upon development, we removed remaining SU-8 residues with isopropyl-alcohol and dried the wafers with compressed air. During the fabrication of high aspect ratio 25 μm microstructures, we experienced bridge formations between micropillars, which impede flow between each structure, and imperfect development of microwells. As a result, we only used the lowest coverage micropillars (d = 10 μm, w = 40 μm) for our experiments with 25 μm-tall microstructures. For microwell structures, fabrication difficulties in high-aspect ratio features using the lowest coverage mask resulted in features with a measured surface coverage ϕ = 0.54 (d = 23.6 μm, w = 9.4 μm) under characterization using an.

      To check pattern fidelity, height uniformity, and bridge formations between pillars, we characterized the fabricated features using a confocal laser microscope. A profilometer (Dektak) was used to measure the average absolute roughness inherent to SU-8, which did not exceed 10 nm both on the flat and the top of the microstructured surfaces.

TABLE 1. Dimensions of the microstructured surfaces investigated in this study (Figure 1). Feature heights are δ_f = 0.4 μm, 2 μm, 10 μm, and 25 μm.

diameter d (μm)	spacing w (μm)	Type	solid fraction ϕ
-	-	Flat	1
10.0	40	Pillars / Wells	0.04 / 0.96
10.0	10	Pillars / Wells	0.23 / 0.77
10.0	3.0	Pillars / Wells	0.54 / 0.46
30.0	3.0	Pillars / Wells	0.75 / 0.25
23.6	9.4	Wells	0.54

C. Experimental Setup

      Our experimental setup consists of flat and microstructured surfaces mounted on a variable incline, with an angle of inclination θ, submerged in a transparent acrylic tank (25 cm × 12.5 cm

× 25 cm) containing a water/glycerol solution at room temperature. The Newtonian water/glycerol solution consists of 90% glycerol and 10% water by weight, with a density of 1230 kg/m³. Due to the hygroscopic nature of highly concentrated glycerol/water solutions, both the kinematic viscosity and density of the solution decrease over time. Thus, we used an Ostwald viscometer to measure the viscosity of the solution before and after each experiment. The measured viscosity varied from $1.20 \times 10^{-4} m^2/s$ to $1.40 \times 10^{-4} m^2/s$ among different sets of experiments but did not change more than 3% within a single three-hour experiment. In the tank of water/glycerol solution, we placed a silicon wafer with fabricated microstructures and fixed the wafer to the center of the floor. We then rolled spheres down the microstructured wafer until all bubbles present between microstructures were removed.

For the experimental measurements, we released silicon nitride spheres individually on the wafer and recorded videos as the spheres rolled down the microstructured surface. We surveyed a range of θ varying from 6 degrees to 30 degrees. For each release, we placed the sphere ~1 cm before the field of view of the camera, with the sphere oriented so that the two parallel lines drawn on the sphere (see Figure 1) were facing the camera. Under this setup, the sphere reaches terminal velocity and steady-state motion practically instantaneously (~ 0.3 sec.) [38,39]. Using a video camera (Apple iPhone 6), we recorded the motion of the sphere at 60 fps, with a resolution of 1080p (1920 × 1080 pixels). We then transferred the videos to a computer and used MATLAB to extract individual frames of each video, then used ImageJ software to analyze the rotational and translational displacements. We calculated the rotational velocity by counting the number of frames required to complete a 90-degree or 180-degree rotation, and we calculated the translational velocity by measuring the displacement at 10 regular intervals as the sphere completes 90-degree or 180-degree rotation. During the calculation, we compared the velocities at each of the 10 intervals to ensure that terminal velocity is achieved. We emphasize that because we determined rotational velocities from angular orientations and translational velocities from displacements, the two velocities are independent measurements, although taken from the same videos. Based on the translational velocities, the particle Reynolds number did not exceed 5×10^{-2} for the 3.00 mm particle and did not exceed 4×10^{-1} for the 5.00 mm particle, even at an angle of inclination of 30 degrees. Hence, noting that the Reynolds numbers are small yet finite, we analyze our results in the Stokes flow limit. The Hersey number, $\lambda = \eta u/P$, defined as the product of the dynamic viscosity, η, and translational velocity, v, divided by the applied normal load, P, was on the order of 1 m⁻¹, varying slightly depending on angle of inclination and sphere size [40,41].

Upon measuring translational and rotational velocities, we calculated fitted effective gap widths, δ_{eff}, and coefficients of friction, μ_{f}, between the sphere and the microstructured substrate for all of our experiments using a least-squares fit following our previous work [32]. The non-linear least-squares fit employed a grid-search method to find the effective gap and coefficient of friction pair of smallest error [42]. The parameter grid surveyed 2800 logarithmically spaced points from 10^{-11} m to 1.5×10^{-4} m for effective gap widths and 150 linearly spaced points from 0.01 to 0.40 for effective coefficients of friction. For each effective gap and coefficient of friction pair, we calculated predicted dimensionless rotational and translational velocities. Then, we computed the square sum of errors in velocities based on these predicted values to identify the fitted effective gap width and coefficient of friction. We compute error bars by propagating the standard deviation of dimensionless velocities and calculating the apparent gap widths that correspond to the error range of velocities.

To clarify our notations, we briefly summarize here the various dimensional gaps that are used throughout this work. δ_{pred} denotes the predicted effective gap based on the dimensions of microstructures, computed using our model in Eq. (12). δ_{eff} represents fitted effective gap based on experimental velocities. δ_{f} and δ_{s} pertain to the dimensions of the actual microstructures. δ_{f} is the height of the fabricated microstructures, measured using a profilometers. δ_{s} is the inherent roughness of SU-8, fitted using experimental velocities of spheres rolling on a flat surface. We emphasize here that all these quantities are dimensional.

D. Sliding Friction Measurements

For the sliding lubricated friction measurements, we used a custom-built multifunctional force microscope (MFM) [43]. In the MFM, forces are calculated from the normal and lateral deflection of a cantilever as measured via fiber optic sensors. The motion of the cantilever is controlled normally by a linear micro-translation stage and a piezoelectric actuator. For a given measurement, the sample is held in place in a fluid bath, which can be moved laterally by a microtranslation stage. A custom-designed LabVIEW platform collects the microtranslator position and cantilever deflection with corresponding a normal spring constant of 1021 N/m and lateral spring constant of 2098 N/m. The probe contacting the surfaces was a 5.00 mm diameter silicon nitride sphere, identical to the ones used in rolling experiments, immobilized on a glass window with epoxy resin and held by the MFM cantilever. Each surface was immobilized in the fluid bath and then covered with a ~1mm layer of fluid (water/glycerol mixture). We then lowered

the cantilever, bringing the sphere into contact with the sample until a 5 mN setpoint was reached. Upon reaching the set point, the sample bath was then moved laterally at a specified velocity over a scan length of 4 mm for several scans. After several trace-retrace repeats, we collected lateral force measurements over four full trace-retrace loops to compute the coefficient of friction. We maintained the normal force setpoint of 5 mN within ±0.2 mN by using a force feedback loop that minimally adjusted the normal microtranslator position for the duration of each experiment.

We performed pure sliding measurements for two different Hersey numbers: 0.0017 m^{-1} and 0.045 m^{-1}. To vary the Hersey number, we probed the surfaces at two different sliding velocities and used a different viscosity fluid for each velocity. To achieve a Hersey number of 0.0017, we used a lateral velocity of 50 μm/s in a glycerol-water mixture identical to that used in rolling experiments. For the Hersey number of 0.045, we used a lateral velocity of 250 μm/s in pure glycerol. The coefficient of friction for each surface was calculated by dividing the lateral force by the applied normal force at each time step. The reported coefficients of friction are the average of four successive traces and retraces that occurred in the middle of a run. In all runs, the surface was traced and retraced at least once before and after the averaged scans to avoid discontinuity associated with initializing and stopping motion.

IV. RESULTS AND DISCUSSION
A. Effect of feature height on the rolling velocity
1.Control experiments in the limit of dilute pillars

First, we aim to validate our general experimental approach by performing control experiments with spheres rolling on surfaces decorated with dilute arrays of pillars to the predictions of Smart *et al*. [24] The data in Figure 2 shows the velocities of 5.00 mm particles down a surface decorated with micropillar arrays of identical, dilute coverage ($\phi = 0.04$), but with different pillar heights. In Figure 2, we also plot dimensionless velocities and draw solid lines from Eqs. (1) – (3) using effective gap widths and coefficients of friction fitted from a least-squares fit. Error bars, which are generally smaller than markers on each data point, represent a standard deviation calculated from four repeats conducted within a single experiment. A video showing a clear difference in sphere velocities on microstructures of $\delta_f = 0.4$ μm and $\delta_f = 25$ μm side-by-side is available in Movie 1 [44]. Experiments on microwells are not considered here because microwells with a dilute area fraction ($\phi < 0.093$) cannot be achieved due to geometric constraints.

Experiments in the dilute limit are in agreement with the work of *Smart et al.* for all microstructure height investigated [24]. First, characteristic dependences on the inclination angle are expected and observed in the velocity plots shown in Figure 2 [24,32]. First, at low inclination angles, the sphere follows a purely rotating motion ($\Omega = U$). Then, as the inclination angle increases and reaches the critical angle, there is a mix of rotation and slipping, resulting in a typical branching of the velocity plots. Finally, as the angle of inclination further increases beyond the critical inclination angle the slipping motion starts to dominate, thereby altering the mode of motion from rotation-dominated to sliding-dominated. As seen in Figure 2, these characteristics are observed for the sphere motion on the three pillar heights surfaces investigated. Also, as expected, our experiments show a very strong effect of the feature height on the velocities of rolling spheres (Ω and U) at low angles when sliding is absent. In particular, we observe an approximately 50% increase in the average non-sliding dimensionless velocity from 0.112 (left) to 0.167 (right) at low angles when the microstructure height increases from 0.4 μm to 25 μm. The critical angle θ_c, shows a small dependence on microstructure heights, implying a dependence of coefficient of friction between the sphere and the incline for the three pillar heights. We also observe that increasing the pillar heights significantly shifts the whole velocity curves upwards, which can be understood in terms of an increasing effective fluid gap, δ_{eff}, between the sphere and the incline. As a final control we see that fitted gaps from our experimental results are in good agreements with independently measured feature heights of the micropatterned pillars. For microstructure heights of $\delta_f = 0.4$ μm, 2 μm, and 25 μm, the obtained fitted gaps were respectively $\delta_{eff} = 0.43$ μm, 2.4 μm, and 17 μm.
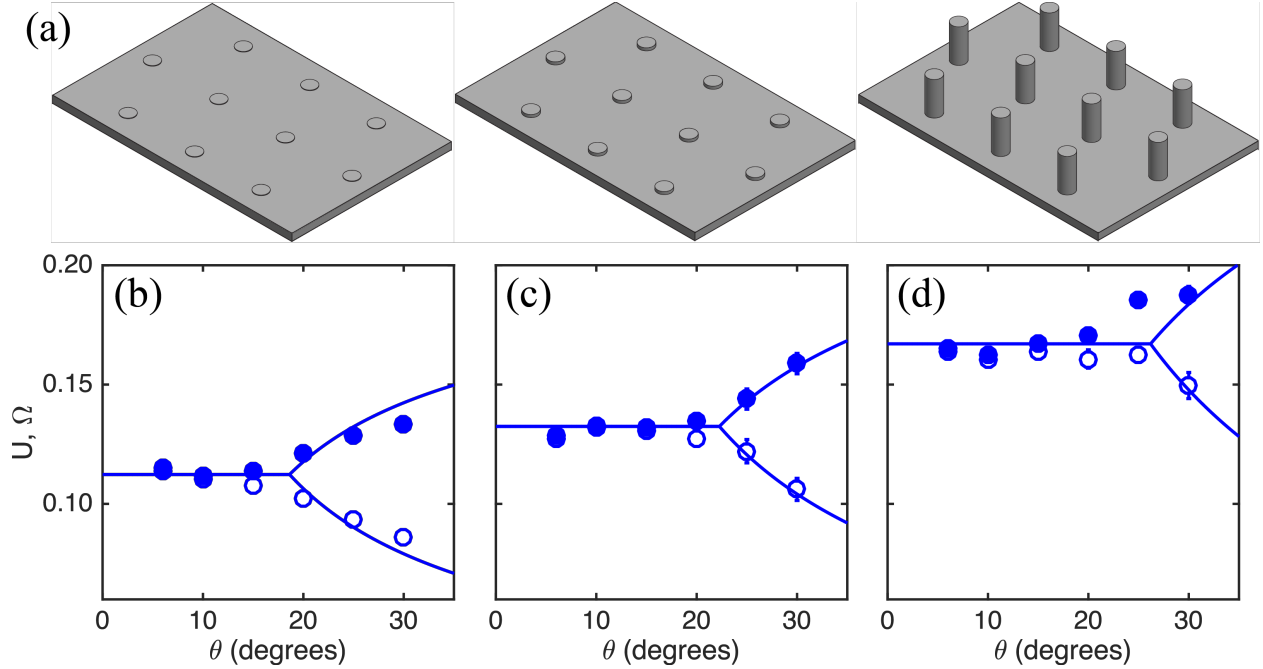
FIG 2. (a) Schematic representation of microstructures and (b-d) experimental dimensionless translational (U, filled markers) and rotational (Ω, open markers) velocities plotted against the angle of inclination, θ, for the 5.00 mm particle. The micropillar arrays have $d = 10$ μm and $w = 40$ μm and are in the dilute limit ($\phi = 0.04$) with heights of (b) $\delta_f = 0.4$ μm , (c) $\delta_f = 2$ μm, and (d) $\delta_f = 25$ μm (right). The solid lines are drawn from eqs. (12) using the fitted gaps, δ_{eff}, and coefficients of friction, μ_f, from a least-squares fit. The effective gaps obtained from the fit were for (b) 0.43 μm, (c) 2.4 μm, and (d) 17 μm.

2. Effective Fluid Gap Width on Non-Dilute Microstructures

In this subsection, we compare experimental results to our model for solid fraction beyond the dilute limit using Eq. (12). We proposed previously that the effective fluid gap width experienced by a rolling sphere can be predicted using a simple linear superposition of the hydrodynamic resistances. Figure 3 shows a comparison between the predicted gaps (Eq. (12)) and the experimentally observed effective gaps (fitted to Eqs (2) – (3)) over all aspect ratios studied. The measurements are performed with surfaces patterned with arrays of either micropillars or microwells, and for four feature heights, δ_f. The black solid lines represent the predicted gaps, calculated using the actual feature heights for each surface δ_f and the inherent surface roughness of SU-8 experienced by particles (δ_s, determined from rolling measurements on a flat surface). The data points show fitted effective gap widths δ_{eff} calculated from our rolling experiments as a function of solid area fraction.

Despite the first-order nature of our model, the experimentally fitted effective gaps from experimental results show excellent agreement with the predictions over all heights and surfaces

studied. As discussed previously, we obtain effective heights that are approximately equal to the feature height at the dilute limit ($\phi = 0.04$) for all four heights investigated (also see Figure 2). For a given feature height, as ϕ increases the effective gap, δ_{eff}, decreases in a power-law manner. At $\phi = 0.96$, δ_{eff} is approximately equal to the inherent surface roughness of SU-8 experienced by particles, δ_{s}. The agreement between predictions and experiment persist even for microstructure heights as low as 0.4 μm (the inherent roughness of our SU-8 layers is approximately ≈ 0.08 μm), as seen in Figure 3(d), regardless of the nature of the microstructure (wells vs. pillars). Although a more refined model might be required to resolve the effect of particle size, our model successfully captures the power-law behavior of the fitted effective gaps. The accuracy of our model at high δ_{f} over all surface coverages suggests that further raising the microstructure height will be able to increase the velocity of rotating spheres.
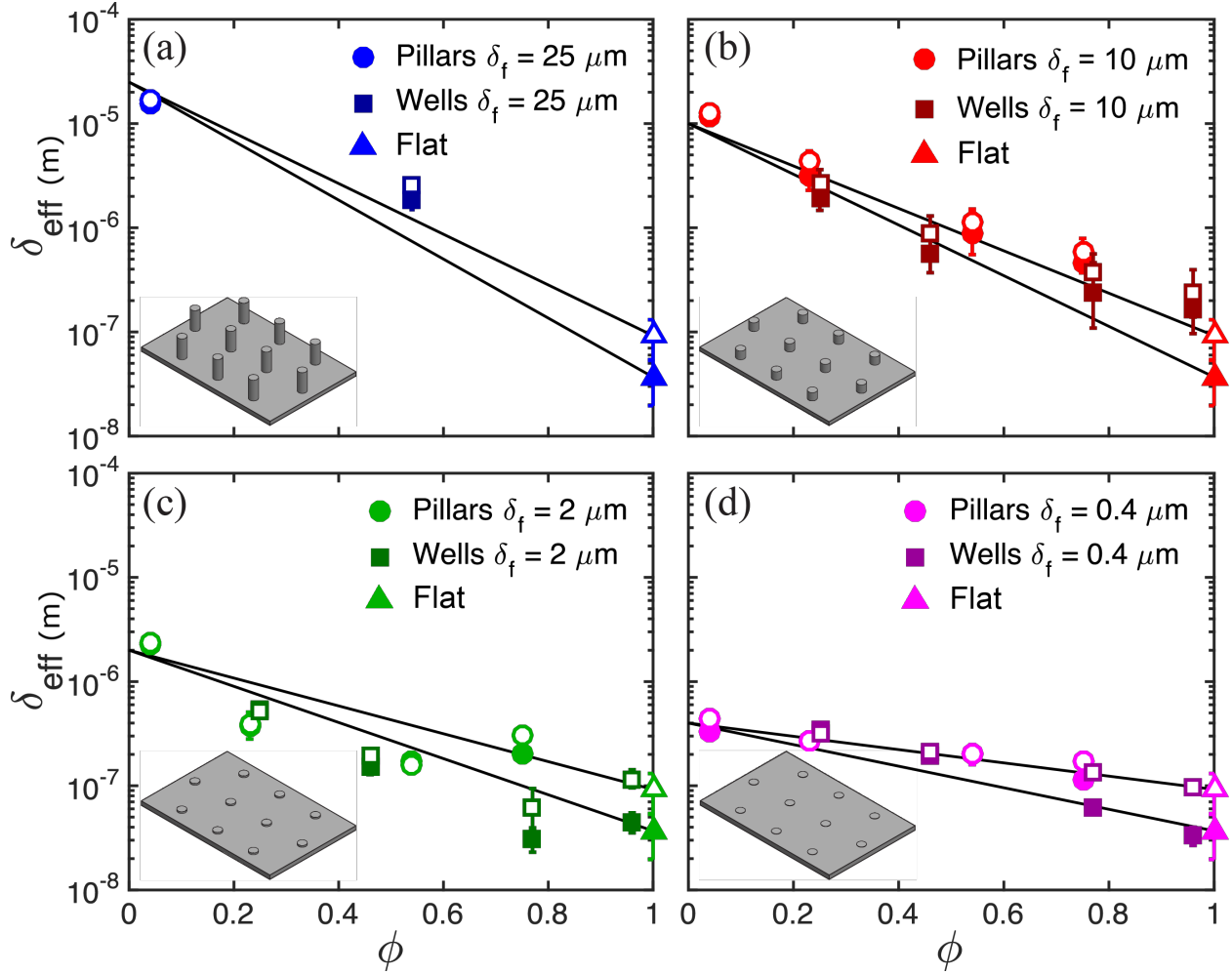

FIG 3. Effective gap widths δ_{eff} fitted from rolling spheres on pillars (circles) and wells (squares), and flat (triangles) surfaces of different heights δ_{f} as a function of microstructure area fraction ϕ. Filled markers

indicate data points obtained from 3.00 mm spheres and open markers indicate data points obtained from 5.00 mm spheres. Error bars represent propagated standard deviations from dimensionless velocities. Solid lines represent predicted gaps from eq (12), connecting δ_f and δ_s for each particle size. The top solid line corresponds to 5.00 mm spheres and bottom solid line corresponds to 3.00 mm spheres. The respective microstructure heights are (a) $\delta_f = 25$ µm, (b) $\delta_f = 10$ µm, (c) $\delta_f = 2$ µm, and (d) $\delta_f = 0.4$ µm. The surface roughness of SU-8 experienced by spheres are $\delta_s = 92$ nm for 5 mm particles, and $\delta_s = 37$ nm for 3mm particles.

Based on exact solutions of hydrodynamic resistance forces and torques by O'Neill and Majumdar, the theoretical limit of dimensionless non-sliding velocities of spheres rotating down an incline is 0.429, when the gap width between the sphere and the incline is large [45]. Future experiments involving alternative fabrication techniques such as silicon etching that overcome soft lithography limitations may elucidate the motion of spheres down extremely tall microstructures [46].

3. Predict Rotational Velocity on a Microstructured Surface

Having an experimental data set that span a range of feature heights allow us to test whether the model can estimate the rolling velocities *a priori* without any fitting parameters. In particular, the model can provide an estimate of the velocities of spheres rolling at low angles of inclinations solely based on the surface roughness δ_s, feature height δ_f, and feature solid area fraction ϕ. We highlight that once these three parameters are known, the prediction can be made *a priori* without further fitting or manipulation of parameters. The data points in Figure 4 represent average velocities, U_{avg}, of spheres at small inclination angles such that the spheres do not slide (i.e. translational and rotational velocities are roughly equal). We used a criterion of $\Omega/U > 0.85$ to determine whether the particle is purely rotating. The solid lines in Figure 4 represent non-sliding velocities U_{avg} predicted from superposition of resistance forces and torques as functions of microstructure height (the model does not differentiate between micropillars and microwells).
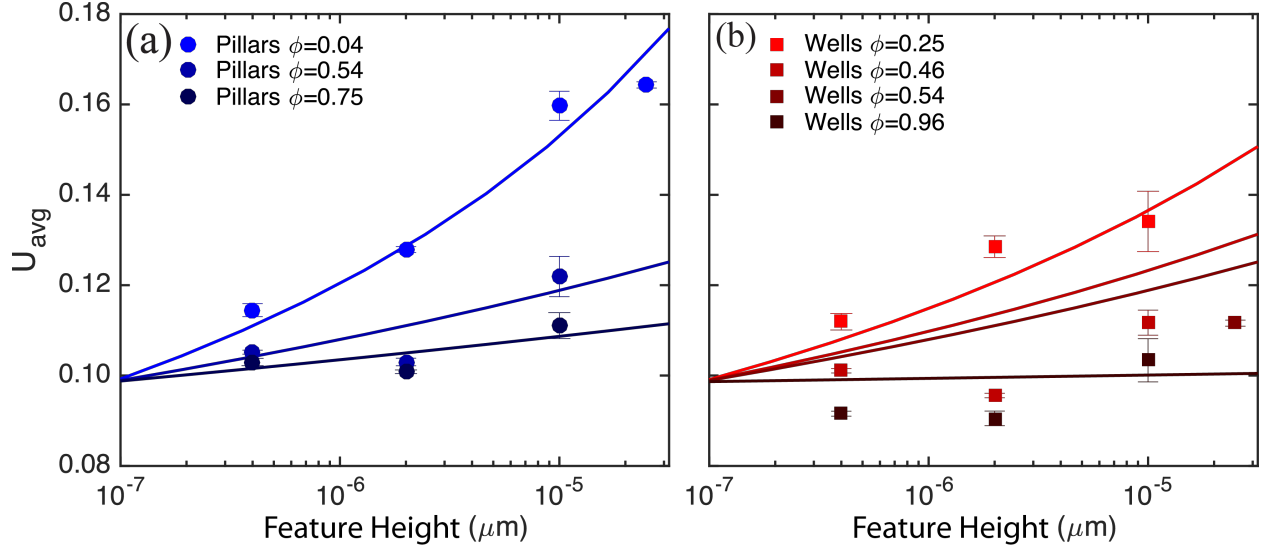
FIG 4. Dimensionless translational velocity U_{avg}, as a function of microstructure height δ_f on (a) micropillars and (b) microwells. U_{avg} is obtained from the average value of the translational velocity over all angles at which spheres purely rotate (i.e. $\theta < \theta_c$ and not sliding). $\Omega/U > 0.85$ was used as a criterion for non-sliding when selecting data points to be averaged. Error bars represent pooled standard deviation of velocities. Solid lines represent predicted dimensionless velocities calculated from eqs. (1) – (3) and eq. (12).

The measured increase in non-sliding velocity with feature height δ_f shows good general agreement with our predictions from eq. (12) for micropillars, and to a lesser extent for microwells (Figure 4). As expected, we observe a strong dependence of sphere velocities on microstructure height δ_f. We also see that the prediction provides a fairly accurate approximation of measured velocities even at non-dilute solid area fraction. Our model predicts that velocities increase with increasing δ_f, and that this dependence on feature height is stronger for microstructures of lower solid area fraction. Hence, the velocities of spheres rolling on arrays of microwells of $\phi = 0.96$ are nearly constant over all δ_f studied. The better prediction for the rotational velocity on micropillars may be due to the presence of interconnected channels. Our treatment assumes an effective plane between the sphere and the incline, therefore the lack of interconnected channels with the microwells may hinder fluid flow between the two surfaces, resulting in quantitative deviations from predicted effective separations. However, we do see agreement in the qualitative trends, especially for wells of low solid area fractions, as spheres are still able to experience the resistance arising from the bottom of microstructures for surfaces of low ϕ. Examination of errors show that the larger error between the experimental values and the predicted ones is due to an increase in sensitivity to perturbations in velocities at smaller effective gaps (i.e. high ϕ and low microstructure height). Since predicted sphere velocities are smaller at low microstructure heights,

the same absolute experimental error in velocity measurements propagate to larger errors in effective gaps when the gaps are smaller.

B. Friction on microstructured surfaces

1. Coefficient of Friction from Rolling Measurements

We now focus on the second parameter we obtain from analyzing the rolling motion of a sphere down an incline, the effective coefficient of friction, μ_f, which our model does not predict. Here, we attempt to better understand how the effective coefficient of friction depends on the microstructure dimensions. Figure 5 shows the dependence on the coefficient of friction on the patterned feature height δ_f obtained from our experiments with rolling spheres of 3.00 mm diameter (the results are similar for the 5.00 mm spheres). For microstructures consisting of either wells or pillars we find that the coefficient of friction generally decreases when the solid area fraction increases. The differences between coverages appear to diminish with increasing height, especially for the surfaces decorated with microwells.
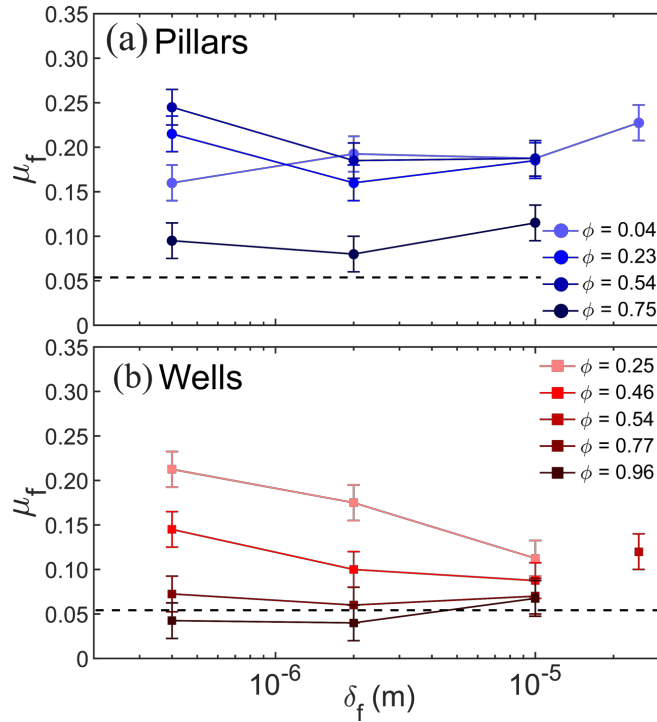

FIG 5. Effective coefficients of friction μ_f of the 3.00 mm rolling spheres as a function of microstructure height δ_f on (a) micropillars, and (b) microwells. The dashed line indicates the friction value on a flat surface. The error bars have a fixed magnitude of 0.02. This values approximately translates to a difference in critical angle of 2 degrees, which provides a conservative range of the variability of dimensionless velocities. Only

one point exists for wells corresponding to $\phi = 0.54$ at $\delta_f = 25$ μm due to difficulties in fabrication of high-aspect ratio microstructures (see Materials and Methods).

A comparison between the coefficient of friction on micropillar (Figure 5(a)) and microwell surfaces (Figure 5(b)) shows that at similar coverages, friction is higher on micropillars than on microwells. The difference in the coefficient of friction between the two types of microstructures is most pronounced at solid area fractions of approximately $\phi \approx 0.50$. Studies on wet friction of bioinspired surfaces suggest that the presence and ease of liquid flow within the microstructure might promote more solid contact between sliding surfaces, thereby increasing friction for surfaces with wider channels between structures [47]. Our results in Figure 5 show that for microwell structures with low ϕ the coefficient of friction tends to be lower for surfaces of higher feature heights, as seen in Figure 5(b). However, we observe a transition for wells with high area fraction ϕ, where the dependence of friction on microstructure height vanishes or even slightly increase with feature height. The dependence of the fitted coefficient of friction on feature heights for microwell structures could be the result of differences in Hersey number within the mixed lubrication regime of a Stribeck curve. The spheres move at higher velocities on taller microstructures, increasing the Hersey number, which should result in a lower coefficient of friction [12]. A decrease in friction at higher sliding velocities on microstructures is consistent with previous tribological studies on microstructured surfaces [48]. These results indicate that the coefficient of friction between a microstructured surface and rotating sphere does depend on the surface structure and therefore cannot be due to simple solid-solid contact, as treated in prior work. Instead, the apparent coefficient of friction must incorporate some contribution from the fluid.

The motions of the spheres are affected by both the fitted effective gap δ_{eff} and the coefficient of friction μ_f. For example, an increase in feature height (δ_f) results in higher effective fluid gap width (δ_{eff}, see Figure 3) and lower coefficient of friction (μ_f, see Figure 5). As a result, their combined contributions lead to a lower rotational velocity Ω and a higher translational velocity U at inclination angles past the critical angle, as shown from the experimental data in Figure 6. The data points show the dependence of the mode of motion in the form of the fraction of rotation in the net translational velocity, Ω/U, on surfaces with a microstructure height of δ_f at two angles of inclination. As predicted, at low angles of inclinations ($\theta = 6°$) we observe purely rotational motion ($\Omega/U = 1$), regardless of microstructure type and area fraction. However, at $\theta = 30°$, Ω/U shows a strong dependence on the microstructure. For both pillars and wells, higher solid area fraction, ϕ, results in more slipping (i.e. lower Ω/U) in general, except at the lowest structure

height and ϕ. Moreover, pillars consistently promote more rotation (higher Ω/U) than wells at an equivalent ϕ over all heights. Finally, we generally observe that the fraction of rotation at a given angle of inclination is lower at higher feature height, especially for microwells. Therefore, we deduce that the highest friction, or greatest amount of rolling, can be achieved on tallest micropillars of low area fraction, while the most slippage is obtained on short microwells of high area fraction.
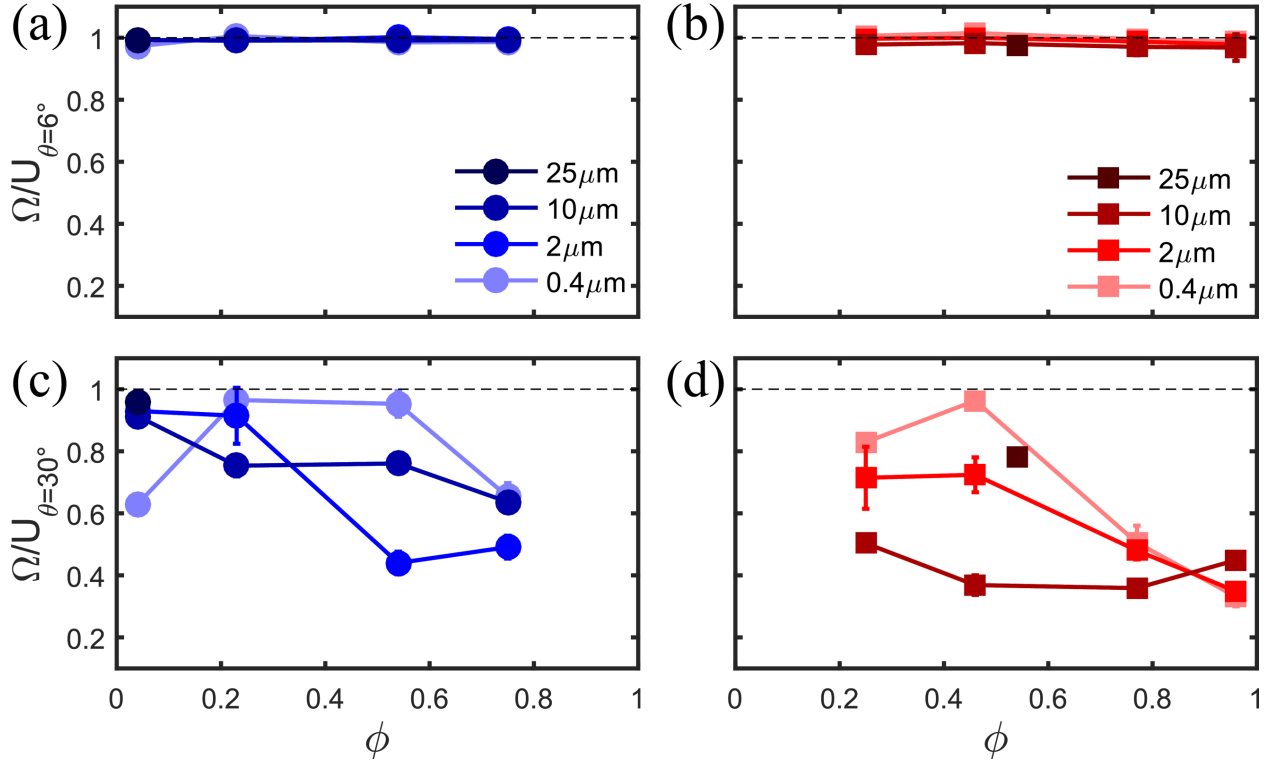

FIG 6. Fractions of rotation in the net translational velocity Ω/U of 3.00 mm sphere on (a) micropillars at θ = 6°, (b) microwells at θ = 6°, (c) micropillars at θ = 30°, and (d) microwells at θ = 30°. The error bars represent standard deviations of fractions of rotations.

2. Importance of Hersey number on the coefficient of friction on microstructured surfaces

Friction regimes are often discussed in the context of Stribeck curves where the coefficient of friction is plotted as a function of the Hersey number ($\lambda = \eta u/P$) [49]. At low Hersey numbers, the coefficient of friction is dominated by boundary contact (solid-solid contacts), which gives a high coefficient of friction. In the other limit, at a high Hersey number the hydrodynamic regime is reached, and the load is supported by the lubricating fluid. In between these two limiting cases lie the mixed lubrication regime at intermediate Hersey numbers, where the load is supported by

both solid-solid contacts and the fluid, and the coefficient of friction is between the one corresponding to the boundary and hydrodynamic regimes, especially for non-conformal contacts [50,51].

We measured the sliding coefficient of friction with the same fluid and material pairs but at significantly lower Hersey numbers that those obtained during the rolling measurements described in the previous section. Our objective is to compare the coefficient of friction measured during sliding to those obtained via rolling (Figures 7 – 9). For the sliding friction measurements, the Hersey numbers were $1.7 \times 10^{-3}\ m^{-1}$ and $4.5 \times 10^{-2}\ m^{-1}$, while for the rolling experiments $\lambda \sim 1\ m^{-1}$ (varying slightly between different angles of inclination and particle sizes). For the sliding measurements, typical trace and retrace curves are shown in Figure 8. As previously mentioned, as a first order approximation we assume that the coefficients of rolling and sliding friction are equal.

We first compare the Stribeck curves for the microstructured surfaces with feature heights of 2 μm (Figure 7). We find, as expected, that decreasing the Hersey number leads to higher coefficients of friction (up to 0.55, while the values obtained from the rolling measurements are between 0.04 and 0.25. For the flat surface we see that the coefficient of friction decreases by an order of magnitude when the Hersey number increases from $1.7 \times 10^{-3}\ m^{-1}$ to $4.5 \times 10^{-2}\ m^{-1}$, which could be due to a transition from boundary to hydrodynamic lubrication. Increasing the Hersey number further to 1 m^{-1} does not decrease the coefficient of friction further. We can then compare the Stribeck curves of the microstructured surfaces to the one obtained with the flat surface. First, we see that at the lowest Hersey number all the microstructured surfaces have similar coefficients of friction, except for the surface decorated with dilute pillars (solid fraction, $\phi = 0.04$). The large coefficient of friction could be dominated by boundary contact. The lower coefficient of friction for the surface with dilute pillars could indicate that even at $\lambda = 1.7x10^{-3}\ m^{-1}$ the surfaces are still in the mixed lubrication regime due to the sparsity of the microstructural features. Then, as the Hersey number increases, the influence of surface geometry emerges as hydrodynamics plays a more important role. First, for the intermediate Hersey number ($\lambda = 0.045$ m^{-1}) the presence of a microstructured surface, microwells or micropillars, significantly increases the friction coefficient (compared to a flat surface). We also find that increasing the Hersey number to $\lambda = 0.045$ m^{-1} leads to a much sharper decrease in the coefficient of friction for the microwell surfaces than for the micropillar surfaces. The interconnected nature of the micropillar surface allows the fluid to drain through the structure and appears to extend the mixed

lubrication regime to much higher Hersey numbers. As a result, the difference in the coefficient of friction between the micropillars and the microwells becomes more pronounced as the Hersey number increases. Such an observation is consistent with prior work, where an increase in friction on microstructured surfaces was attributed to fluid drainage through the structure favoring boundary contact [52,53].
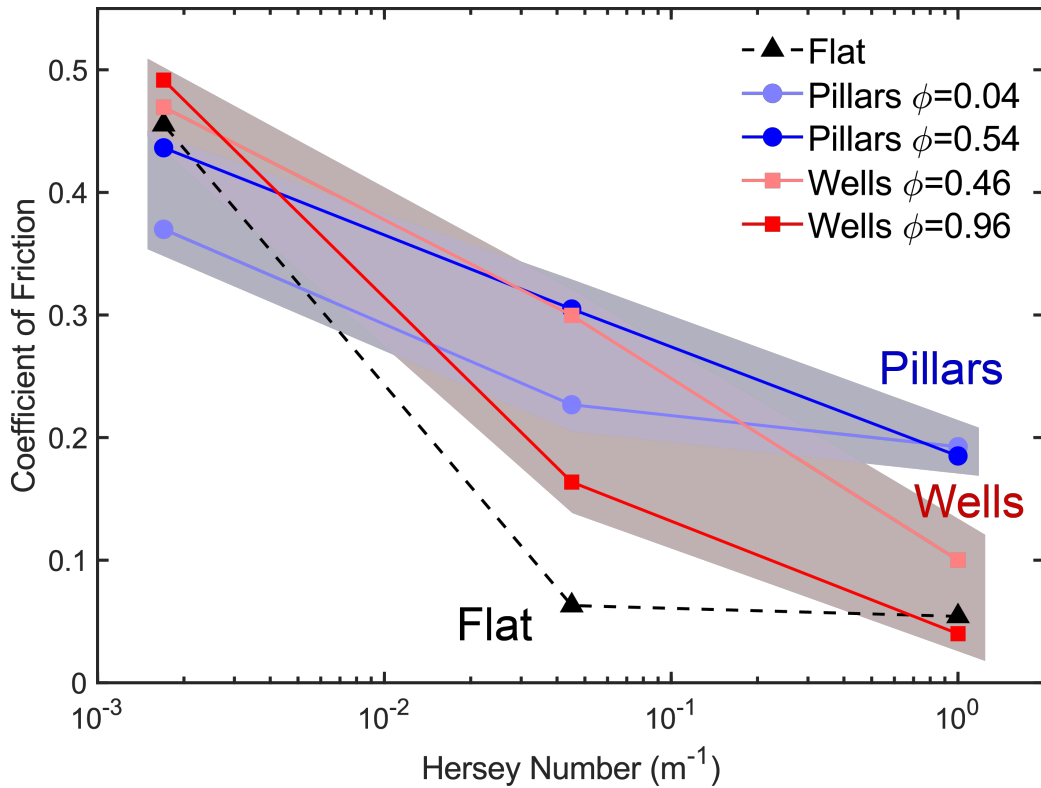

FIG 7. Coefficients of friction on flat and microstructured surfaces shown as a function of Hersey number ($\lambda = \eta u / P$). The shaded regions allow for a visual comparison between the Stribeck curves of pillars and wells. The coefficients of friction at Hersey numbers $\lambda \sim 1\ m^{-1}$ are obtained from the rolling experiments with 3mm and 5mm Si_3N_4 spheres. The coefficients of friction at lower Hersey numbers are obtained from sliding friction measurements.
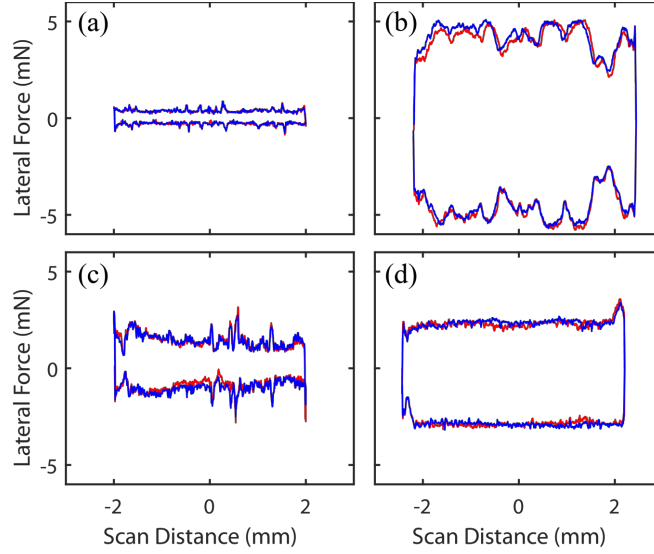
FIG 8. Typical friction loops for structured surfaces obtained using a multifunction force microscope. Sliding friction measurements shown for (a) – (b) smooth surface at H = 0.045 and H = 0.0017, respectively, and (c) – (d) 25 µm 10x40 pillars at H = 0.045 and H = 0.0017, respectively. For each friction coefficient the force measurements from four traces and retraces were averaged, we display two complete loops for clarity. Red curves represent the first of four averaged loops and blue curves represent the second. All friction loops were similar for a given surface and Hersey number.
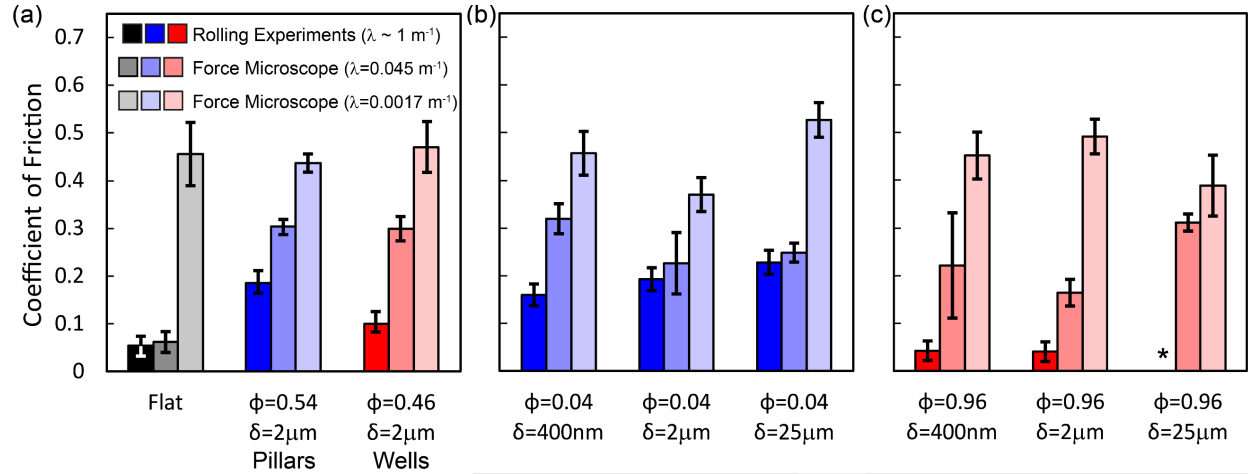

FIG 9. Comparison of coefficients of friction measured from rolling experiments (dark bars) and force microscopes of two different Hersey Numbers λ (intermediate and light bars) for different surface coverages ϕ and microstructure height δ. Error bars show standard deviation of coefficient of friction within a sliding experiment. Friction corresponding to rolling experiments on $\phi = 0.96$ and $\delta = 25$ µm in (c), denoted as *, is unavailable.

We also find that for an identical solid areal fraction, for $\lambda=0.045$ m^{-1} the type of microstructure (wells vs pillars) leads to similar coefficients of friction, even if the microwells do not allow for fluid drainage (Figures 7 and 9(a)). In the high Hersey number regime obtained from rolling measurements ($\lambda \sim 1\ m^{-1}$), we see that surfaces decorated with micropillars have a higher

coefficient of friction compared to surfaces decorated with microwells. In addition, the surfaces decorated with microwells have a comparable coefficient of friction than the flat surface. Finally, we see that the Hersey number has a more pronounced effect on the friction than the effect of microstructure height (Figures 9(b)-(c)). Our experiments clearly demonstrate that the role of the microstructures in modulating the coefficient of friction can have opposite effect depending on the Hersey number. We also see that the nature of the microstructured surface (wells vs pillars) has a more pronounced effect on friction at higher Hersey numbers.

Our measurements demonstrate that rolling spheres could be used to characterize the tribological properties of microstructured surfaces. The results in Figures 7 – 9 show that simply analyzing the rotational and translational velocities of rolling spheres can probe high Hersey number regimes at low loads, a regime that can be difficult to attain using a tribometer due to sensitivity limitations. Yet, future experiments should be performed to verify whether the presence of rotational motion in rolling experiments affects the coefficient of friction, because the analysis assumes that coefficients of rolling and sliding frictions are equal. Studies involving particles with geometries that can purely slide, such as a flat disk, or by comparing rolling experiments and sliding force measurements at equivalent Hersey numbers could answer these questions.

V. CONCLUSION

We investigated how the various design parameters of engineered microstructured surfaces impact the motion of a sphere rolling down a structured plane incline in a viscous environment. We monitored the rolling motion of silicon nitride spheres on silicon wafers patterned with either micropillar or microwell arrays of varying surface coverage ($\phi = 0.04$ to $\phi = 0.96$), and feature height (aspect ratios from 0.04 to 2.5). We captured videos of the rolling spheres to independently examine their rotational and translation velocities, and to analyze and model their motion using the contact-force model developed by Smart *et al*. [24] Furthermore, we conducted a separate series of sliding friction measurements to investigate the role of the Hersey number on the coefficient of friction for the microstructured surfaces.

Our experimental results showed good quantitative agreement with the predictions provided by our model over all microstructure heights studied. The model, based on superposition of hydrodynamic resistance forces and torques from the top and bottom plane of microstructures, succeeds in providing an effective separation between the sphere and the plane incline for microstructures of heights varying over two orders of magnitude and all surface coverages. Based

on this approximation we can predict the rolling velocity of spheres at low inclination angles without any fitting parameters.

We then characterized the coefficient of friction on microstructured surfaces across three orders of magnitude in the Hersey number to identify the design parameters determining the coefficient of friction. We found that the role of the microstructure became more significant in determining the coefficient of friction with increasing Hersey number. At low Hersey number where the mode of friction was mainly boundary contact there were little differences in the coefficient of friction. As the Hersey number increased, the coefficient of friction for all surfaces decreases, but more so for surfaces decorated with microwells. Our experiments appear to indicate that the mixed lubrication regime is extended up to higher Hersey numbers for surfaces decorated with micropillars than for flat or microwells surfaces. At the highest Hersey number, during the rolling experiments, we observed a strong correlation between the surface coverage and the friction coefficient, where the friction decreased as the coverage of the microstructures increased. Hence, spheres mainly rotated on microstructures of low coverages, whereas spheres slipped considerably on surfaces of high microstructural coverages. Furthermore, arrays of micropillars, which allow fluid flow between each feature, exhibited higher friction compared to microwell arrays that act as isolated cells of fluid. Therefore, we can conclude that the greatest fraction of rolling can be achieved with dilute micropillars of small heights, whereas the greatest slippage is obtained on tall microwells of high area fraction.

Finally, these results demonstrate the ability to measure coefficients of friction based on the rotational and translational velocities of rolling spheres and suggests that this method of incorporating a video camera can be further developed as a simple, non-destructive technique that can probe the friction properties of the surface. This technique may be utilized in the characterization of various microstructured surfaces for microfluidic and industrial applications at which a non-destructive means of studying tribological properties are required at a high Hersey number regime.

ACKNOWLEDGEMENTS

REFERENCES

[1] S. N. Gorb, M. Sinha, A. Peressadko, K. A. Daltorio, and R. D. Quinn, Bioinspiration Biomim. **2**, S117 (2007).

[2] Y. Zhou, A. Robinson, U. Steiner, and W. Federle, J. R. Soc., Interface **11**, 20140499 (2014).

[3] M. Varenberg and S. Gorb, J. R. Soc., Interface **5**, 383 (2008).

[4] S. N. Gorb, Am. Entomol. **51**, 31 (2005).

[5] G. Hanna and W. J. P. Barnes, J. Exp. Biol. **155**, 103 (1991).

[6] W. Federle, W. Barnes, W. Baumgartner, P. Drechsler, and J. Smith, J. R. Soc., Interface **3**, 689 (2006).

[7] B. Persson, J. Phys.: Condens. Matter **19**, 376110 (2007).

[8] M. R. Cutkosky and S. Kim, Philos. Trans. R. Soc., A **367**, 1799 (2009).

[9] D. Gropper, L. Wang, and T. J. Harvey, Tribol. Int. **94**, 509 (2016).

[10] C. Gachot, A. Rosenkranz, S. Hsu, and H. Costa, Wear **372**, 21 (2017).

[11] C. Greiner, M. Schäfer, U. Popp, and P. Gumbsch, ACS Appl. Mater. Interfaces **6**, 7986 (2014).

[12] L. Galda, P. Pawlus, and J. Sep, Tribol. Int. **42**, 1505 (2009).

[13] A. Kovalchenko, O. Ajayi, A. Erdemir, G. Fenske, and I. Etsion, Tribol. Int. **38**, 219 (2005).

[14] M. Scaraggi, F. P. Mezzapesa, G. Carbone, A. Ancona, and L. Tricarico, Tribol. Lett. **49**, 117 (2013).

[15] A. Mongruel, T. Chastel, E. S. Asmolov, and O. I. Vinogradova, Phys. Rev. E **87**, 011002 (2013).

[16] T. Chastel and A. Mongruel, Phys. Fluids **28**, 023301 (2016).

[17] G. A. Pilkington, R. Gupta, and J. l. Fréchette, Langmuir **32**, 2360 (2016).

[18] M. Scaraggi, Phys. Rev. E **86**, 026314 (2012).

[19] C. Myant, H. Spikes, and J. Stokes, Tribol. Int. **43**, 55 (2010).

[20] M. Guingo and J.-P. Minier, J. Aerosol Sci. **39**, 957 (2008).

[21] K.-C. Chang, D. F. Tees, and D. A. Hammer, Proc. Natl. Acad. Sci. U. S. A. **97**, 11262 (2000).

[22] D. A. Hammer and S. M. Apte, Biophys. J. **63**, 35 (1992).

[23] A. López-Cervantes, I. Dominguez-Lopez, J. D. O. Barceinas-Sanchez, and A. L. García-García, J Mech Behav Biomed Mater. **20**, 45 (2013).

[24] J. R. Smart, S. Beimfohr, and D. T. Leighton Jr, Phys. Fluids A **5**, 13 (1993).

[25] Y. Zhao, K. P. Galvin, and R. H. Davis, Int. J. Multiphase Flow **28**, 1787 (2002).

[26] A. Maali, Y. Pan, B. Bhushan, and E. Charlaix, Phys. Rev. E **85**, 066310 (2012).

[27] B. He, W. Chen, and Q. J. Wang, Tribol. Lett. **31**, 187 (2008).

[28] H. Yu, W. Huang, and X. Wang, Lubr. Sci. **25**, 67 (2013).

[29] H. Yu, H. Deng, W. Huang, and X. Wang, Proc. Inst. Mech. Eng., Part J **225**, 693 (2011).

[30] R. Berthé, G. Westhoff, H. Bleckmann, and S. Gorb, J. Comp. Physiol., A **195**, 311 (2009).

[31] Y. Kim, Y. Chung, A. Tsao, and R. Maboudian, ACS Appl. Mater. Interfaces **6**, 6936 (2014).

[32] B. K. Ryu, C. Dhong, and J. Fréchette, Langmuir **33**, 164 (2017).

[33] W. Dean and M. O'Neill, Mathematika **10**, 13 (1963).

[34] M. E. O'Neill, Mathematika **11**, 67 (1964).

[35] A. J. Goldman, R. G. Cox, and H. Brenner, Chem. Eng. Sci. **22**, 637 (1967).

[36] K. Galvin, Y. Zhao, and R. Davis, Phys. Fluids **13**, 3108 (2001).

[37] M. E. Staben, K. P. Galvin, and R. H. Davis, Chem. Eng. Sci. **61**, 1932 (2006).

[38] M. Jalaal and D. Ganji, Powder Technol. **198**, 82 (2010).

[39] C.-D. Jan and J.-C. Chen, J. Hydraul. Res. **35**, 689 (1997).

[40] M. D. Hersey, J. Wash. Acad. Sci. **4**, 542 (1914).

[41] M. Woydt and R. Wäsche, Wear **268**, 1542 (2010).

[42] C. Ritz and J. C. Streibig, *Nonlinear regression with R* (Springer Science & Business Media, 2008).

[43] P. Roberts, G. A. Pilkington, Y. Wang, and J. Frechette, Rev. Sci. Instrum. **89**, 043902 (2018).

[44] See Supplemental Material at (URL to be inserted by publisher).

[45] M. E. O'Neill and R. Majumdar, Z. Angew. Math. Phys. **21**, 164 (1970).

[46] L. Sainiemi, T. Nissilä, V. Jokinen, T. Sikanen, T. Kotiaho, R. Kostiainen, R. A. Ketola, and S. Franssila, Sens. Actuators, B **132**, 380 (2008).

[47] H. Chen, L. Zhang, D. Zhang, P. Zhang, and Z. Han, ACS Appl. Mater. Interfaces **7**, 13987 (2015).

[48] T. Khosla, J. Cremaldi, J. S. Erickson, and N. S. Pesika, ACS Appl. Mater. Interfaces **7**, 17587 (2015).

[49] X. Lu, M. Khonsari, and E. Gelinck, J Tribol **128**, 789 (2006).

[50] M. Kalin, I. Velkavrh, and J. Vižintin, Wear **267**, 1232 (2009).

[51] H. Spikes, Lubr. Sci. **9**, 221 (1997).

[52] M. Varenberg and S. N. Gorb, Adv. Mater. **21**, 483 (2009).

[53] D. M. Drotlef, L. Stepien, M. Kappl, W. J. P. Barnes, H. J. Butt, and A. del Campo, Adv. Funct. Mater. **23**, 1137 (2013).